Rapid Communications

Emergence of a ferromagnetic insulating state in $LaMnO_3/SrTiO_3$ heterostructures: Role of strong electronic correlations and strain

Hrishit Banerjee* and Markus Aichhorn

Institute of Theoretical and Computational Physics, Graz University of Technology, NAWI Graz, Petersgaße 16, A-8010 Graz, Austria

(Received 23 March 2020; revised manuscript received 26 May 2020; accepted 15 June 2020; published 24 June 2020)

Inspired by the experimental findings of an exotic ferromagnetic insulating state in $LaMnO_3/SrTiO_3$ (LMO/STO) heterostructures, we calculate the electronic and magnetic state of $LaMnO_3/SrTiO_3$ superlattices with comparable thicknesses employing *ab initio* dynamical mean-field theory. Projecting on the low-energy subspace of Mn 3*d* and Ti 3*d* states, and solving a multi-impurity problem, our approach emphasizes local correlations at the Mn and Ti sites. We find that a ferromagnetic insulating state emerges due to the intrinsic effects of strong correlations in the system, in agreement with experimental studies. We also predict that, due to electronic correlations, the emerging two-dimensional electron gas is located at the LMO side of the interface. This is in contrast to density-functional theory results that locate the electron gas on the STO side. We estimate the transition temperature for the paramagnetic-to-ferromagnetic phase transition, which may be verified experimentally. Importantly, we also clarify that the epitaxial strain is a key ingredient for the emergence of the exotic ferromagnetic insulating state. This becomes clear from calculations on a strained $LaMnO_3$ system, also showing ferromagnetism which is not seen in the unstrained bulk material.

DOI: 10.1103/PhysRevB.101.241112

Introduction. Since the first report of a highly conducting and mobile two-dimensional electron gas (2DEG) occurring at the interface of oxide insulators [1], the study of heterointerfaces formed between perovskite oxides has had a serious impact on the scientific community engaged in experimental and computational condensed matter research. It has paved the way for many different prospective device applications, and garnered considerable interest in the field of oxide electronics. Interfaces have been formed between band insulators, for example, between $SrTiO_3$ (STO) and $LaAlO_3$ (LAO) [1,2], and between band insulators and Mott insulators, as in the case of $SrTiO_3$ and $GdTiO_3$ (GTO) [3,4], with qualitatively different behavior from that of the LAO/STO interface. This is due to the fact that $GdTiO_3$, being a Mott insulator, has a very different band structure compared to LAO which is a band insulator, which in turn has a deep influence on the band alignment of the two oxides making up the interface [5].

Experimental studies on interfaces between cooperative Jahn-Teller (JT) distortion-driven insulators such as $LaMnO_3$ (LMO), in which strong correlations have a significant effect, with band insulators such as $SrTiO_3$ have been carried out in the recent past. In these systems, the interplay of structural distortions and strong electronic correlations is expected to lead to a variety of different phases. Indeed, large and diverse numbers of magnetic and electronic phases of the LMO/STO interfaces have been observed, depending on the relative thickness of STO and LMO and their geometry [6–12]. Among these varied numbers of electronic and magnetic states, the most intriguing is the observation of ferromagnetic insulating behavior, which has been reported for both LMO/STO superlattices and thin-film/substrate geometries when LMO and STO have comparable thicknesses [10,12]. Since ferromagnetism is generally associated with metallicity, and antiferromagnetism is typically seen in the case of insulators, this happens to be a counterintuitive observation.

Ferromagnetic insulators are essential for many new magnetic devices, such as dissipationless quantum-spintronic devices, magnetic tunneling junctions, etc. Ferromagnetic insulators with a high T_C and a high-symmetry crystal structure are required for interfacing with single-crystalline oxide films or substrates. The few known high-symmetry materials either have extremely low Curie temperatures ($\leqslant$16 K) [13,14], or require chemical doping of an antiferromagnetic matrix. Thus, it is imperative to theoretically understand the origin of intrinsic ferromagnetic insulating behavior in heterostructures.

Few attempts have been made in the case of LMO/STO to theoretically justify the observed coexistence of ferromagnetism and insulating properties. Most of these attempts depend on either symmetry lowering or on orbital polarization effects. However, symmetry lowering in the geometry of strained LMO [15] seems unlikely in superlattices because LMO is sandwiched between cubic STO. Concerning orbital polarization, experiments show a significant suppression of the JT distortion, further supported by density-functional theory (DFT + U) studies [16,17], which in turn reduces orbital polarization [12] in the superlattice geometry that hosts the ferromagnetic insulating behavior. A further attempt suggests electronic phase separation leading to the nucleation of metallic nanoscale ferromagnetic islands embedded in an insulating antiferromagnetic matrix. This, however, is not the case for

*h.banerjee10@gmail.com

intrinsic ferromagnetic insulating behavior [10]. The observed coexistence of ferromagnetism and insulating behavior in the LMO/STO heterostructure thus remains a mystery.

Banerjee *et al.* studied the problem considering bulk LMO, but epitaxially strained to the lattice constants of a square substrate of STO [17], within Hartree-Fock (HF) based hybrid functional calculations. They find a ferromagnetic insulating ground state driven by the marked reduction of orthorhombic distortion in the optimized strained LMO structure, resulting in a strong suppression of the JT distortion. This suppression and the modification of the octahedral rotation are in agreement with the structural characterization of LMO/STO superlattices [12]. The insulating behavior was attributed to originate from electronically driven charge disproportionation within the Mn sublattice that arises due to a strain-driven enhanced covalency between Mn and O. However, charge disproportionation has yet to be confirmed experimentally.

The questions that we intend to address in this Rapid Communication are thus well defined. We are interested in looking at how strong correlations affect these oxide LMO/STO heterostructure systems. In particular, we intend to examine the fate of the 2D electron gas. We carry out paramagnetic density-functional theory (DFT) plus dynamical mean-field theory (DMFT) calculations on $(LMO)_{2.5}/(STO)_{2.5}$ and $(LMO)_{3.5}/(STO)_{2.5}$ which are multi-impurity calculations including both Ti $3d$ and Mn $3d$, and observe a metal-to-insulator phase transition by varying the interaction strength. Furthermore, we also find a ferromagnetic insulating solution which is stable at low enough temperatures. Both heterostructures, $(LMO)_{2.5}/(STO)_{2.5}$ and $(LMO)_{3.5}/(STO)_{2.5}$, yield qualitatively similar results. In contrast to previous studies, we find that the 2D electron gas generated due to the polar catastrophe moves to the LMO side of the interface and effectively dopes the Mn $3d$ orbitals.

An important result of our study is that a ferromagnetic insulating state emerges also in a calculation of a bulk $LaMnO_3$ system, which is strained to match the square STO substrate. As $LaMnO_3$ at ambient pressure is antiferromagnetic, this opens up a way to induce phase transitions between different magnetic states as a function of strain. This may be realized by modern experimental techniques of stress generation.

Computational details. We perform the DMFT calculations in a basis set of projective Wannier functions, which were calculated using the TRIQS/DFTTOOLS package [18–22]. For paramagnetic calculations, only Mn t_{2g} orbitals have been considered for the DMFT calculation, while for ferromagnetic calculations all five Mn d orbitals have been taken into account to allow for high-spin solutions. In all calculations we included the Ti t_{2g} orbitals as being correlated. The Anderson impurity problems were solved using the continuous-time quantum Monte Carlo algorithm in the hybridization expansion (CT-HYB) [23] as implemented in the TRIQS/CTHYB package [24]. We performed one-shot calculations, with the double-counting correction treated in the fully localized limit [25]. We used the rotationally invariant Kanamori interaction [26]. For our calculations we used U values ranging from 4.5 to 8 eV and J varying between 0.5 and 0.75 eV to investigate the metal-to-insulator transition. We set the intraorbital interaction to be $U' = U - 2J$. Real-frequency results have been obtained using the maximum-entropy method of analytic continuation as implemented in the TRIQS/MAXENT application [27].

The problem of unstrained bulk $LaMnO_3$ has been widely studied in the literature and it is well known that a large value of static effective Hubbard U is required in DFT + U methods to account for the experimentally observed band gap of the A-type antiferromagnetic (AFM) insulating state. For instance, a large value of effective $U = 8$ eV was required to obtain a band gap of 1.4 eV [28]. A previous study shows that calculations using hybrid functionals with HF exchange of 25% yield a value of 1.7 eV band gap [17]. We want to note that the actual value of the band gap of bulk LMO is also not clear experimentally. There is a rather large distribution of values, ranging from 1.1 [29], over 1.7 [30] and 1.9 [31], up to 2.0 eV [32,33].

LMO/STO superlattice. We investigate the electronic structure of LMO on STO in the experimental setup, i.e., we consider a heterostructure consisting of LMO and STO layers. In addition to the square epitaxial strain generated due to the mismatch between the LMO and STO unit cells, the superlattices in particular involve the polar discontinuity formed between LMO consisting of alternating layers of LaO and MnO_2 of $+1$ and -1 charges, respectively, and STO consisting of alternating charge neutral layers of SrO and TiO_2. The latter would cause half a charge to be transferred between the layers at the interface. Neither the direction nor extent of this charge transfer have been clarified. We consider superlattice geometries of LMO/STO, with an alternate repetition of LMO and STO layers of comparable thickness, stacked along the [001] direction. This creates two symmetric n-type interfaces between the LaO layer of LMO and the TiO_2 layer of STO [5,12,17]. The structure of the superlattice for the case of $(LMO)_{3.5}/(STO)_{2.5}$ has been shown in the top panel of Fig. 1. Comparable thicknesses are chosen since the FM insulating

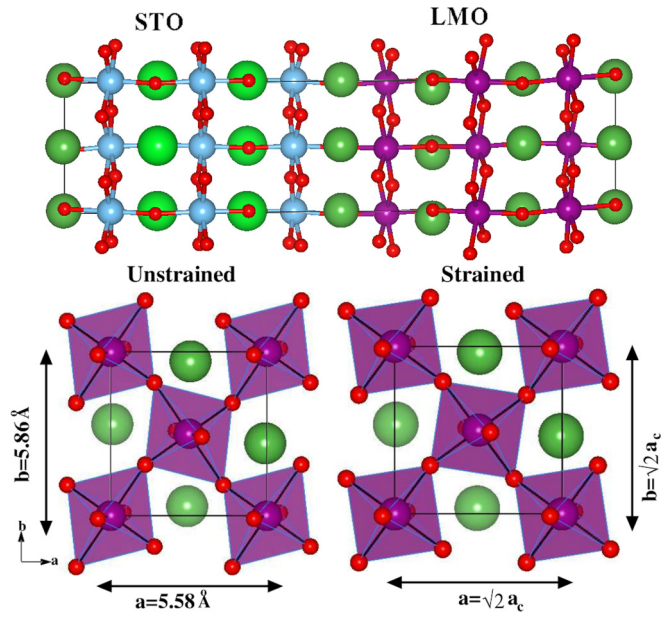

FIG. 1. Top: $(LMO)_{3.5}/(STO)_{2.5}$ superlattice, with two symmetric n-type interfaces. Bottom: Unstrained and epitaxially strained LMO when the lattice constants of LMO are matched to an STO lattice.

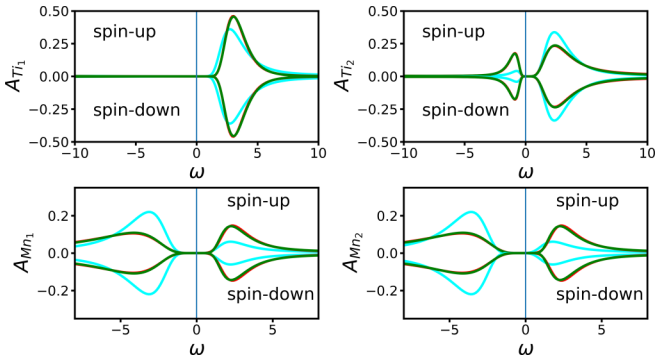

FIG. 2. Spectral functions for Ti t_{2g} [d_{xy} (cyan), d_{yz}(red), d_{xz} (green)] and Mn t_{2g} (color is the same as for Ti) orbitals showing the paramagnetic insulating phase at $\beta = 40$ eV^{-1}. Ti_1, Ti_2, Mn_1, Mn_2 belong to different inequivalent layers of the $(LMO)_{3.5}/(STO)_{2.5}$ superlattice and form the four impurities of the system.

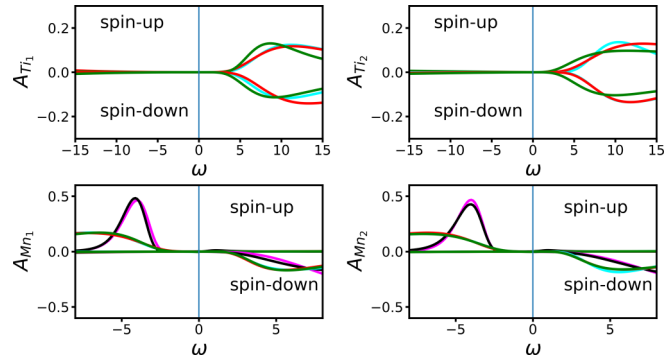

FIG. 3. Spectral functions for Ti t_{2g} [d_{xy} (cyan), d_{yz} (red), d_{xz} (green)] and Mn d [$d_{x^2-y^2}$ (magenta), d_{z^2} (black), and color for t_{2g} the same as in the case of Ti] orbitals showing a FM insulating phase at $\beta = 60$ eV^{-1}. Ti_1, Ti_2, Mn_1, Mn_2 labeling is the same as Fig. 2.

state has been experimentally observed for superlattice geometries with a nearly equal thickness of LMO and STO layers [12]. In this Rapid Communication, we show multi-impurity calculations for heterostructure systems, which are not very common in existing literature.

For the structural relaxation, we place LMO in an orthorhombic geometry matching the square plane of STO layers (in the [100] and [010] directions). Here, a $\sqrt{2} \times \sqrt{2} \times c$ supercell of both LMO and STO was allowed to tilt and rotate. This results in four Mn and Ti atoms in each MnO_2 and TiO_2 layer, respectively. The ionic positions and c lattice parameters are allowed to relax, keeping the constraint on the planar lattice constants of $a = b$. This generates a square-matched epitaxial strain of -1.8%. The optimized structure shows a significant decrease in JT distortion, and modification of tilt and rotation angles in LMO, while some JT distortion, and tilt and rotation is introduced in the STO due to its proximity to the distorted LMO block. This is very similar to other heterostructures such as GTO/STO [5].

Our paramagnetic DFT calculations reveal a metallic solution with Ti t_{2g} and Mn t_{2g} states at the Fermi level. We first carry out paramagnetic DMFT calculations at $\beta = 40$ eV^{-1}, including Ti t_{2g} and Mn t_{2g} orbitals. We use $U = 6$ eV and $J = 0.75$ eV on Ti t_{2g}, and $U = 8$ eV and $J = 0.75$ eV on Mn t_{2g}. This gives an insulating solution with a band gap of $\sim$2 eV seen in the spectral function, as shown in Fig. 2. The insulating state may be driven to a metallic state by reducing the value of U on Mn to below $U = 6$ eV.

In the next step, in order to account for a spin-polarized solution [18], we first extend the Wannier basis set to include all 3d orbitals of Mn to allow for the high-spin state of Mn with a magnetic moment of $4\mu_B$. Starting from the paramagnetic solutions, we introduce a spin splitting in the real part of the self-energies and let the DMFT iterative cycle converge to a possibly spin-split solution. We carry out the calculations at various values of β between 40 and 80 eV^{-1}. At $\beta = 40$ eV^{-1}, the calculation converges still to a paramagnetic state, but when reducing the temperature we find a transition to a ferromagnetic ground state. The spectral function at $\beta = 60$ eV^{-1} is shown in Fig. 3. We see a clear splitting between the up- and down-spin channels, and a reasonably large band gap.

What is very interesting to note is that the Ti t_{2g} orbitals are now completely emptied out whereas the occupancies of the Mn d orbitals are $\sim$4.5 each. This indicates that the electron gas is located at the the LMO side of the interface when correlations are included and properly taken care of. In contrast, previous studies using DFT + U and hybrid functionals put the electron gas at the STO side and explain the insulating behavior of Ti electrons by a high-spin polarization [17]. However, those approaches are inadequate when it comes to capturing the correct nature of the correlations. From our calculations, however, we can show from an actual first-principles calculation the doping of Mn due to the 2DEG, arising purely from correlation effects. Though this has been suggested before [10] and used to propose a superparamagnetic state (ferromagnetic puddles in an antiferromagnetic matrix) instead of an actual intrinsic ferromagnetic insulating state, explicit calculations showing this doping of LMO did not exist.

Next, we look at the temperature dependence of the ferromagnetic solution. Since for this purpose a larger number of calculations at different temperatures are required, we are doing calculations for a $(LMO)_{2.5}/(STO)_{2.5}$ heterostructure. This structure is obtained from $(LMO)_{3.5}/(STO)_{2.5}$ as shown in Fig. 1 by removing one LMO layer. Hence, this reduces the number of inequivalent Mn atoms from two to one, leading to a three-impurity DMFT problem and hence making calculations cheaper. Importantly, $(LMO)_{2.5}/(STO)_{2.5}$ shows essentially the same qualitative electronic structure as $(LMO)_{3.5}/(STO)_{2.5}$. We plot the Wannier magnetic moments on Mn, obtained from the density matrix of the spin-split DMFT solution, in Fig. 4. It is obvious that a transition from a paramagnetic to a ferromagnetic state occurs at around $\beta = 60$ eV^{-1}, which corresponds roughly to a temperature of 200 K. Given the fact that DMFT overestimates strongly the magnetic transition temperatures [34], we would give a rough estimate for the transition temperature T_C to be around 50–100 K. A more precise prediction is beyond the capabilities of single-site DMFT calculations. We note that the Néel temperature for bulk unstrained LMO has been measured experimentally to be $\sim$177 K. We also note that our saturated magnetic moment is enhanced to $\sim 4.9\mu_B$, instead of $4\mu_B$ as expected for Mn with a d^4 configuration. This enhancement comes from the two symmetric n-type interfaces giving 0.5e

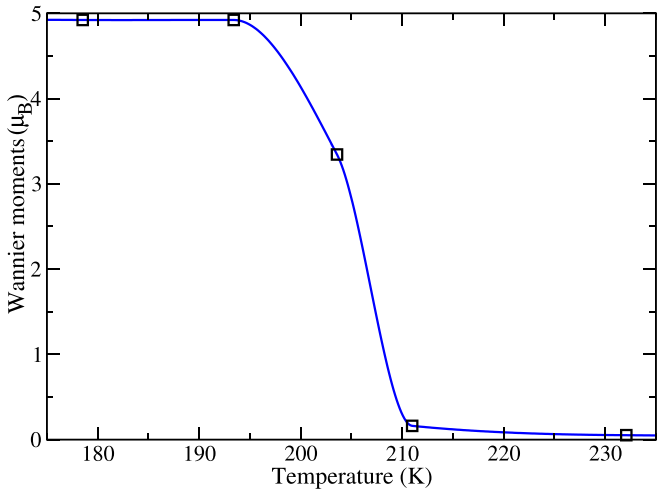

FIG. 4. Plot of Wannier magnetic moments of Mn as a function of temperature.

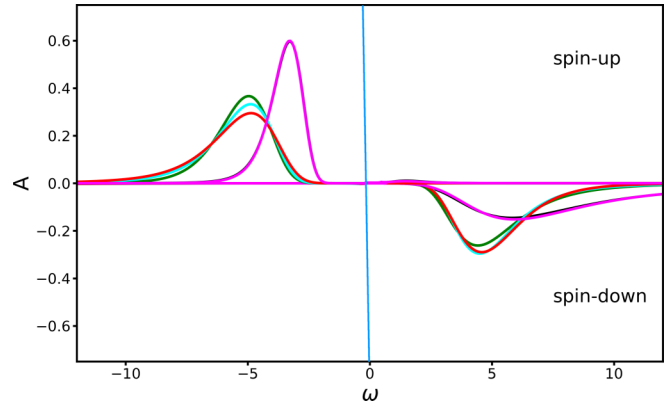

FIG. 5. Spectral functions for epitaxially strained LMO, Mn d [d_{xy} (cyan), d_{yz} (red), d_{xz} (green), $d_{x^2-y^2}$ (magenta), d_{z^2} (black)] at $\beta = 60$ eV^{-1}. We observe a ferromagnetic phase with a clear spin splitting.

each to the 2DEG. This again confirms that the electron generated due to polar catastrophe moves to the LMO side of the interface and dopes the Mn atoms instead of the Ti atoms. When discussing heterostructure systems the natural question arises on how to manipulate the heterostructures to increase the T_C of the system. However, this is a delicate task, since many parameters such as the size of the magnetic moment, coupling constants, gap size, etc., contribute to T_C [34]. Interestingly, there is a recent study of LMO/$SrMnO_3$ heterostructures with a ferromagnetic T_C of up to 350 K [35].

Epitaxially strained LMO. In this final part, we want to clarify the role of strain on the magnetic state, and whether the heterostructure geometry is necessary for it. This we do by looking at bulk LMO samples.

Bulk unstrained LMO crystallizes in the orthorhombic *Pbnm* crystal structure, and is an *A*-type antiferromagnetic insulator. In order to mimic the effect of epitaxial strain, we carry out "strained bulk" calculations. The structural parameters (c lattice parameter and ionic positions) of the orthorhombic perovskite unit cells are optimized under the constraint that the two in-plane lattice vectors, defining the epitaxial substrate, are kept fixed to produce the specific square lattice corresponding to the substrate, in our case that of STO. The lower panel of Fig. 1 shows the structure of unstrained and strained LMO, viewed along the c direction. We find a rather strong influence of strain on the structural parameters of LMO, particularly on the JT distortion, which becomes negligibly small in the case of a compressive strain of 1.8% generated by an STO substrate with $a_c = 3.905$ Å. A strong reduction of tilt and rotation of the octahedra is also seen due to the epitaxial strain of the square substrate.

Paramagnetic DFT + DMFT calculations with interaction values $U = 6$ eV and $J = 0.75$ eV yield an insulting ground state at $\beta = 40$ eV^{-1}. As for the heterostructure calculations, we then try to find a spin-split solution by introducing a spin splitting to the paramagnetic solution. By doing so, we find a ferromagnetic insulator with a net magnetization of $M = 3.96\mu_B$ at $\beta = 60$ eV^{-1}. The spectral function for this ferromagnet is shown in Fig. 5. If we decrease β slightly, there is a phase transition to a $M = 0\mu_B$ paramagnetic insulating phase at $\beta = 50$ eV^{-1}. Thus, we obtain here a very similar T_C as in the previous case of the LMO/STO heterostructures.

We thus conclude that our DFT + DMFT calculations based on a five-orbital d model yield a ferromagnetic insulator within a reasonable range of interaction parameters for epitaxially strained LMO as well, a phase which is not seen in the bulk unstrained condition of LMO. The necessary strain may be generated experimentally very easily by modern piezoelectric methods of strain generation as recently demonstrated by Hicks *et al.* [36].

Summary and discussion. With the aim of providing an understanding of the ferromagnetic insulating state in LMO/STO heterostructures, we apply *ab initio* DFT + DMFT methods to both superlattices of LMO/STO and strained bulk LMO structures.

We investigated the case of LMO/STO superlattice structures with comparable thicknesses of LMO and STO. The ground state was found to be insulating in both paramagnetic and ferromagnetic DFT + DMFT calculations. In all heterostructure geometries that we considered, the 2DEG was found to reside on the LMO side of the interface, contrary to DFT results. Though this has been suggested before, this is the first time that an actual first-principles calculation shows the doping of Mn due to the 2DEG. We also showed that the transition temperature from the paramagnetic to ferromagnetic phase is high enough to be of practical relevance and accessible to experimental studies.

Finally, we showed that epitaxial straining of LMO to the square substrate of STO is key for the ferromagnetic ground state. This primarily results from a strong suppression of the JT distortion, which quenches the orbital polarization and hence antiferromagnetism in turn. For the "strained bulk" structure, it was found that DFT+DMFT yields a ferromagnetic insulating solution for a small enough temperature. The critical temperature T_C here is similar to the case of the heterostructures.

Since the exotic ferromagnetic insulating state does exist in the case of strained LMO, it may even be realized by using modern piezoelectric experimental techniques for generating uni- and/or biaxial strain. Our study shows from the

perspective of correlation and dynamics, the emergence of the exotic ferromagnetic insulating state, which has been touted to be immensely important in the case of many spintronics applications.

Acknowledgments. This work has been funded by the Austrian Science Fund (FWF), START Project No. Y746. Calculations have been performed on the local cluster network at TU Graz.

[1] A. Ohtomo and H. Y. Hwang, Nature (London) **427**, 423 (2004).
[2] S. Gariglio, N. Reyren, A. D. Caviglia, and J.-M. Triscone, J. Phys.: Condens. Matter **21**, 164213 (2009).
[3] P. Moetakef, T. A. Cain, D. G. Ouellette, J. Y. Zhang, D. O. Klenov, A. Janotti, C. G. Van de Walle, S. Rajan, S. J. Allen, and S. Stemmer, Appl. Phys. Lett. **99**, 232116 (2011).
[4] T. A. Cain, P. Moetakef, C. A. Jackson, and S. Stemmer, Appl. Phys. Lett. **101**, 111604 (2012).
[5] H. Banerjee, S. Banerjee, M. Randeria, and T. Saha Dasgupta, Sci. Rep. **5**, 18647 (2015).
[6] J. Garcia-Barriocanal, J. C. Cezar, F. Y. Bruno, P. Thakur, N. B. Brookes, C. Utfeld, A. Rivera-Calzada, S. R. Giblin, J. W. Taylor, J. A. Duffy, S. B. Dugdale, T. Nakamura, K. Kodama, C. Leon, S. Okamoto, and J. Santamaria, Nat. Commun. **1**, 82 (2010).
[7] J. Garcia-Barriocanal, F. Y. Bruno, A. Rivera-Calzada, Z. Sefrioui, N. M. Nemes, M. Garcia-HernÃ¡ndez, J. Rubio-Zuazo, G. R. Castro, M. Varela, S. J. Pennycook, C. Leon, and J. Santamaria, Adv. Mater. **22**, 627 (2010).
[8] W. S. Choi, D. W. Jeong, S. S. A. Seo, Y. S. Lee, T. H. Kim, S. Y. Jang, H. N. Lee, and K. Myung-Whun, Phys. Rev. B **83**, 195113 (2011).
[9] H. M. Liu, C. Y. Ma, P. X. Zhou, S. Dong, and J.-M. Liu, J. Appl. Phys. **113**, 17D902 (2013).
[10] Y. Anahory, L. Embon, C. J. Li, S. Banerjee, A. Meltzer, H. R. Naren, A. Yakovenko, J. Cuppens, Y. Myasoedov, M. L. Rappaport, M. E. Huber, K. Michaeli, T. Venkatesan, Ariando, and E. Zeldov, Nat. Commun. **7**, 12566 (2016).
[11] X. R. Wang, C. J. Li, W. M. Lü, T. R. Paudel, D. P. Leusink, M. Hoek, N. Poccia, A. Vailionis, and T. Venkatesan, Science **349**, 716 (2015).
[12] X. Zhai, L. Cheng, Y. Liu, C. M. Schlepütz, S. Dong, H. Li, X. Zhang, S. Chu, L. Zheng, J. Zhang, A. Zhao, H. Hong, A. Bhattacharya, J. N. Eckstein, and C. Zeng, Nat. Commun. **5**, 4283 (2014).
[13] A. Mauger and C. Godart, Phys. Rep. **141**, 51 (1986).
[14] J. H. Lee *et al.*, Nature (London) **466**, 954 (2010).
[15] Y. S. Hou, H. J. Xiang, and X. G. Gong, Phys. Rev. B **89**, 064415 (2014).
[16] J. H. Lee, K. T. Delaney, E. Bousquet, N. A. Spaldin, and K. M. Rabe, Phys. Rev. B **88**, 174426 (2013).
[17] H. Banerjee, O. Janson, K. Held, and T. Saha-Dasgupta, Phys. Rev. B **100**, 115143 (2019).
[18] See Supplemental Material at http://link.aps.org/supplemental/10.1103/PhysRevB.101.241112 for full computational details of the DFT calculations, and a reaffirmation of results where we start with spin-polarized DFT calculations and look at the DMFT solutions thence, which includes the following references: J. P. Perdew, K. Burke, and M. Ernzerhof, Phys. Rev. Lett. **77**, 3865 (1996); P. E. Blöchl, Phys. Rev. B **50**, 17953 (1994); G. Kresse and J. Hafner, *ibid.* **47**, 558(R) (1993); **54**, 11169 (1996); P. Blaha, K. Schwarz, G. K. H. Madsen, D. Kvasnicka, J. Luitz, R. Laskowski, F. Tran, and L. D. Marks, *WIEN2k, An Augmented Plane Wave + Local Orbitals Program for Calculating Crystal Properties* (Karlheinz Schwarz, Technische Universität Wien, Austria, 2018).
[19] O. Parcollet, M. Ferrero, T. Ayral, H. Hafermann, I. Krivenko, L. Messio, and P. Seth, Comput. Phys. Commun. **196**, 398 (2015).
[20] M. Aichhorn, L. Pourovskii, V. Vildosola, M. Ferrero, O. Parcollet, T. Miyake, A. Georges, and S. Biermann, Phys. Rev. B **80**, 085101 (2009).
[21] M. Aichhorn, L. Pourovskii, and A. Georges, Phys. Rev. B **84**, 054529 (2011).
[22] M. Aichhorn, L. Pourovskii, P. Seth, V. Vildosola, M. Zingl, O. E. Peil, X. Deng, J. Marvlje, G. Kraberger, C. Martins, M. Ferrero, and O. Parcollet, Comput. Phys. Commun. **204**, 200 (2016).
[23] P. Werner and A. J. Millis, Phys. Rev. B **74**, 155107 (2006).
[24] P. Seth, I. Krivenko, M. Ferrero, and O. Parcollet, Comput. Phys. Commun. **200**, 274 (2016).
[25] V. I. Anisimov, I. V. Solovyev, M. A. Korotin, M. T. Czyzyk, and G. A. Sawatzky, Phys. Rev. B **48**, 16929 (1993).
[26] J. Kanamori, Prog. Theor. Phys. **30**, 275 (1963).
[27] G. J. Kraberger, R. Triebl, M. Zingl, and M. Aichhorn, Phys. Rev. B **96**, 155128 (2017).
[28] T. A. Mellan, F. Cora, R. Grau-Crespo, and S. Ismail-Beigi, Phys. Rev. B **92**, 085151 (2015).
[29] T. Arima, Y. Tokura, and J. B. Torrance, Phys. Rev. B **48**, 17006 (1993).
[30] T. Saitoh, A. E. Bocquet, T. Mizokawa, H. Namatame, A. Fujimori, M. Abbate, Y. Takeda, and M. Takano, Phys. Rev. B **51**, 13942 (1995).
[31] J. H. Jung, K. H. Kim, D. J. Eom, T. W. Noh, E. J. Choi, J. Yu, Y. S. Kwon, and Y. Chung, Phys. Rev. B **55**, 15489 (1997).
[32] J. H. Jung, K. H. Kim, T. W. Noh, E. J. Choi, and J. Yu, Phys. Rev. B **57**, R11043 (1998).
[33] R. Krüger, B. Schulz, S. Naler, R. Rauer, D. Budelmann, J. Backstrom, K. H. Kim, S.-W. Cheong, V. Perebeinos, and M. Rübhausen, Phys. Rev. Lett. **92**, 097203 (2004).
[34] J. Mravlje, M. Aichhorn, and A. Georges, Phys. Rev. Lett. **108**, 197202 (2012).
[35] M. Keunecke, F. Lyzwa, D. Schwarzbach, V. Roddatis, N. Gauquelin, K. Müller-Caspary, J. Verbeeck, S. J. Callori, F. Klose, M. Jungbauer, and V. Moshnyaga, Adv. Funct. Mater. **30**, 1808270 (2020).
[36] C. W. Hicks, D. O. Brodsky, E. A. Yelland, A. S. Gibbs Jan, A. N. Bruin *et al.*, Science **344**, 283 (2014).